MOLECULAR AND CELLULAR BIOLOGY, Jan. 2009, p. 389–401 Vol. 29, No. 2
0270-7306/09/$08.00+0 doi:10.1128/MCB.00904-08

Contributions of F-BAR and SH2 Domains of Fes Protein Tyrosine Kinase for Coupling to the FcεRI Pathway in Mast Cells▽†

Victor A. McPherson,[1]‡ Stephanie Everingham,[1]‡ Robert Karisch,[1] Julie A. Smith,[1] Christian M. Udell,[1] Jimin Zheng,[1] Zongchao Jia,[1] and Andrew W. B. Craig[1,2]*

Department of Biochemistry, Queen's University, Kingston, Ontario K7L 3N6, Canada,[1] and Queen's University Cancer Research Institute, Division of Cancer Biology and Genetics, Kingston, Ontario K7L 3N6, Canada[2]

Received 6 June 2008/Returned for modification 18 July 2008/Accepted 29 October 2008

This study investigates the roles of Fer-CIP4 homology (FCH)–Bin/amphiphysin/Rvs (F-BAR) and SH2 domains of Fes protein tyrosine kinase in regulating its activation and signaling downstream of the high-affinity immunoglobulin G (IgE) receptor (FcεRI) in mast cells. Homology modeling of the Fes F-BAR domain revealed conservation of some basic residues implicated in phosphoinositide binding (R113/K114). The Fes F-BAR can bind phosphoinositides and induce tubulation of liposomes in vitro. Mutation of R113/K114 to uncharged residues (RK/QQ) caused a significant reduction in phosphoinositide binding in vitro and a more diffuse cytoplasmic localization in transfected COS-7 cells. RBL-2H3 mast cells expressing full-length Fes carrying the RK/QQ mutation show defects in FcεRI-induced Fes tyrosine phosphorylation and degranulation compared to cells expressing wild-type Fes. This correlated with reduced localization to Lyn kinase-containing membrane fractions for the RK/QQ mutant compared to wild-type Fes in mast cells. The Fes SH2 domain also contributes to Fes signaling in mast cells, via interactions with the phosphorylated FcεRI β chain and the actin regulatory protein HS1. We show that Fes phosphorylates C-terminal tyrosine residues in HS1 implicated in actin stabilization. Thus, coordinated actions of the F-BAR and SH2 domains of Fes allow for coupling to FcεRI signaling and potential regulation the actin reorganization in mast cells.

Mast cells reside in connective and mucosal tissues and play a key protective role in the immune response to helminth infection (13, 21), sepsis (39), and snake or bee venoms (42). Mast cells express FcεRI, which becomes sensitized to antigens or allergens upon immunoglobulin E (IgE) binding. Aggregation of FcεRI by multivalent antigens causes the release of preformed mediators by degranulation and the de novo production of lipid mediators and cytokines (1, 52). Release of these mediators causes increased vascular permeability, leukocyte recruitment and activation, and inflammation (41). Aberrant mast cell activation is implicated in IgE-mediated type I hypersensitivity reactions including anaphylaxis, allergic rhinitis, and asthma (20). FcεRI is a tetrameric receptor composed of an IgE-binding α chain and of β and γ chains containing immunoreceptor tyrosine-based activation motifs that become phosphorylated following multivalent antigen-mediated clustering of FcεRI and activation of Src family protein tyrosine kinases (PTKs), primarily involving Lyn (51). Lyn phosphorylates and activates both positive effectors of FcεRI signaling (e.g., Syk PTK) and key negative regulators (e.g., Shp-1 and SHIP) that serve to limit mast cell activation (28, 46, 69).

Fes (the mammalian orthologue of the v-Fps and v-Fes oncoproteins from avian [57, 58] and feline [15, 56] retroviruses) and Fer are closely related PTKs that become activated following FcεRI aggregation in mast cells (10). Surprisingly, FcεRI-induced tyrosine phosphorylation of Fes and Fer does not require their kinase activities (55) and is almost entirely dependent on Lyn (67). Through the use of transgenic mouse models, evidence for both unique and redundant functions for Fes and Fer has been described in regulating hematopoiesis (55) and limiting the innate immune response (22, 40, 50, 72). In mast cells, we have shown that Fer promotes activation of p38 mitogen-activated protein kinase and chemotaxis of mast cells (10). We also found that Fer and Fes PTKs contribute to FcεRI-evoked phosphorylation of platelet-endothelial cell adhesion molecule 1 (PECAM-1) (67).

Each of the Fes and Fer PTKs is composed of an N-terminal regulatory domain containing a Fer-CIP4 homology (FCH) domain followed by several predicted coiled-coils (CC), a central SH2 domain, and C-terminal PTK domain (19). It is worth noting that early studies pointed toward an important role for the N-terminal domain of v-Fps for its transforming activity and membrane localization (5, 63). Several recent studies have defined the FCH and first CC domain (amino acids 1 to 300) in Fer, CIP4, and other *pombe* Cdc15 homology (PCH) family adaptor proteins as an F-BAR domain (also termed extended FCH or EFC domain) (reviewed in references 3 and 9). The F-BAR domain was found to constitute a novel phosphoinositide-binding domain that can promote tubulation of liposomes in vitro and membranes in vivo (27, 33, 66). The crystal structures of F-BAR domains from several PCH adaptors were recently solved (27, 59). The F-BAR module was shown to consist of a triple helical bundle that forms a homodimer, with a concave surface rich in basic residues that have recently been shown to contact phospholipids in curved membranes (16). In vitro studies using the Fer F-BAR domain have shown that the F-BAR domain binds strongly to phosphatidylinositol-4,5-

* Corresponding author. Mailing address: Department of Biochemistry, Queen's University, Kingston, Ontario K7L 3N6, Canada. Phone: (613) 533-2496. Fax: (613) 533-6830. E-mail: ac15@queensu.ca.

‡ V.A.M. and S.E. contributed equally to this work.

† Supplemental material for this article may be found at http://mcb.asm.org/.

▽ Published ahead of print on 10 November 2008.

bisphosphate [PI(4,5)P_2]; however, the Fer F-BAR is relatively weak compared with the adaptor protein FBP17 at inducing membrane tubulation (66). Liposome sedimentation assays have identified several conserved basic residues required for F-BAR domain binding to PI(4,5)P_2(66). The substitution of R113/K114 to glutamines (RK/QQ) in FBP17 reduced phosphoinositide binding by 80% (66). A recent electron cryoelectron microscopy study provided insights into binding of F-BAR dimers to flat and curved membranes via different binding faces (16). This study also confirmed that R113/K114 residues (in CIP4) constitute a site of direct interaction with the liposomes. Interestingly, microdomains of the plasma membrane rich in PI(4,5)P_2 are sites of dynamic actin assembly (47) and endocytosis (4, 31). Previous studies have described Fes localization to a variety of subcellular structures, including endocytic vesicles (71), the *trans*-Golgi apparatus (71), microtubules (37), and focal adhesions (44). The rapid activation of Fes and Fer PTKs upon FcεRI aggregation on mast cells (10) would suggest that there is a mechanism by which Fes localizes at or near the plasma membrane. Phosphoinositide-binding via the F-BAR domain of Fes and Fer PTKs may promote their recruitment to the plasma membrane prior to their activation by cell surface receptors such as FcεRI. The potential colocalization with endocytosis and actin assembly regulators may allow for regulation of receptor endocytosis or chemotaxis of mast cells by Fes/Fer PTKs. A recent study implicates Rab5 GTPase and its exchange factor RabGEF1/Rabex-5 in promoting internalization of FcεRI following clustering by antigens (34). It is worth noting that defects in internalization of Toll-like receptor 4 and transferrin receptor were observed in Fes-deficient macrophages (48), and there is a potential role for Fes in regulating internalization of mast cell receptors.

In this study, we provide novel insights into the phospholipid binding and liposome tubulating properties of the Fes F-BAR domain. Mutation of two conserved basic residues within the Fes F-BAR domain (RK/QQ) reduced phospholipid binding in vitro, and membrane localization in vivo. In transfected RBL-2H3 mast cells, the Fes harboring the RK/QQ mutation ($Fes^{RK/QQ}$) displayed reduced FcεRI-evoked tyrosine phosphorylation compared to wild-type Fes (Fes^{WT}), which correlated with reduced localization to Lyn-containing membranes in mast cells. The SH2 domain of Fes was found to interact with several phosphoproteins in mast cells, including FcεRI and HS1, an actin regulator and cortactin homologue. We found that Fes contributes to HS1 phosphorylation at C-terminal residues implicated in actin branch stabilization, and we present a model for how F-BAR-containing adaptor proteins and PTKs may coordinate actin-driven endocytosis in mast cells.

MATERIALS AND METHODS

Constructs. Retroviral MSCVpac-based (where MSCV is murine stem cell virus and *pac* is the puromycin *N*-acetyltransferase gene) expression plasmids (25) encoding C-terminally Myc epitope-tagged human Fes^{WT} and Fes with the K588R mutation (Fes^{K588R}) were kindly provided by P. Greer (Queen's University). The RK/QQ mutation in Fes was generated using a QuikChange Site-Directed Mutagenesis kit (Stratagene), MSCV-Fes plasmid and the primers (Integrated DNA Technologies Inc. was the source of all primers) 5′-CGGGAACGGCAGCAATTGCAGCAGA CCTACAGCGAGCAGTGG-3′ and 5′-CCACTGCTCGCTGTAGGTCTGCTG CAATTGCTGCCGTTCCCG-3′, which contained an MfeI site for screening. The mutation was verified by sequencing. Plasmids encoding the minimal human Fes F-BAR domain (Fes residues 1 to 300) or an extended construct including F-BAR and the CC2 and CC3 (CC2/3) domains (Fes residues 1 to 459) were generated by PCR amplification from MSCV-Fes plasmids using the EcoRI-containing forward primer 5′-CGGAATTCATGGGCTTCTCTTCCGAGCTG-3′ with either the SalI-containing reverse primer 5′-CGGTCGACCTAGTTCAGCTGGAGCTCCCCAG G-3′ (for residues 1 to 300) or XhoI-containing reverse primer 5′-GTCCTCGAG CACAGCCCTGTGCAGGACAAC-3′ (for residues 1 to 459). Following directional cloning of EcoRI/SalI- or EcoRI/XhoI-digested PCR products and pGEX6P.1, constructs were verified by restriction digestion and sequencing. Using these plasmids as templates, the RK/QQ mutation was conferred as above. The R113E/K114E (RK/EE) mutation was prepared as above, using primers 5′-CCGG GAACGGCAGCAATTGGAAGAGACCTACAGCGAGCAGTGG-3′ and 5′-C CACTGCTCGCTGTAGGTCTCTTCCAATTGCTGCCGTTCCCGG-3′. A construct consisting of green fluorescent protein (GFP) and residues 1 to 300 of Fes [GFP-Fes(1-300)] was generated by ligation of the PCR product described above into pEGFP-C2 digested with EcoRI/SalI. Constructs were verified by restriction digestion and sequencing, and mutagenesis was performed as described above. The SH2 domain of human Fes was expressed as a glutathione *S*-transferase (GST) fusion protein following PCR amplification of MSCV-Fes with primers (5′-GCGG ATCCTGGTACCACGGGGCCATCCCG-3′ and 5′-GCAGCGGCCGCCACAG CCCTGTGCAGGACAAC-3′), digestion with BamHI/NotI, and cloning into pGEX 4T-3. An expression construct for the C-terminal domain of SPY75 (mouse HS1) fused to GST was described previously (17) (here referred to as GST-$HS1_{CT}$), and was kindly provided by T. Kawakami (La Jolla Institute of Allergy and Immunology). Mutations of Y388F and Y405F and a double mutant (Y388F/Y415F) within $HS1_{CT}$ were generated using a QuikChange Site-Directed Mutagenesis kit (Stratagene) with the following primers: Y388Ffor, 5′-CCCGAGCCTGAGAATG AATTCGAGGACGTTGAGGAG-3′; Y405Ffor, 5′-GAACCAGAGGGGGAAT TCGAGGAGGTGCTCGAG-3′; Y388Frev, 5′-CTCCTCAACGTCCTCGAATT CATTCTCAGGCTCGGG-3′; Y405Frev, 5′-CTCGAGCACCTCCTCGAATTCC CCCTCTGGTTC-3′. An EcoRI restriction site encoding silent mutations was created adjacent to Y388/Y405 for screening, followed by verification by sequencing. GST-PECAM-1(CT), encoding the C-terminal tail of PECAM-1 was described previously (67).

GST fusion protein expression and purification. All GST-containing plasmids were transformed into BL21 cells, and colonies were grown in 1-liter cultures of LB medium to mid-log phase and cooled to room temperature, and protein expression was induced using 1 mM isopropyl-β-D-thiogalactopyranoside (IPTG) overnight. Lysates were prepared in buffer A1000 (20 mM Tris, pH 8, 1,000 mM NaCl, 0.2 mM EDTA, 0.5 mM DTT, 0.1% phenylmethylsulfonyl fluoride) supplemented with 150 μg/ml lysozyme, sonicated, and clarified prior to purification using glutathione-Sepharose beads (1 ml) according to the manufacturer's instructions (GE Healthcare Ltd.).

Creation of stable cell lines. MSCVpac (vector) and MSCV-based plasmids encoding Myc-Fes^{WT}, Myc-Fes^{K588R}, and Myc-$Fes^{RK/QQ}$ (20 μg) were transfected by electroporation (310 V, 950 μF) into 10^6 RBL-2H3 cells. Following transfection, cells were cultured with growth medium (Dulbecco's modified Eagle's medium supplemented with 10% [vol/vol] fetal bovine serum, 1% [vol/vol] glutamine, 1% [vol/vol] antimicrobial-antimycotic solution, and 24 μl/ml [vol/vol] nystatin) and incubated at 37°C. After 2 days, transfected cells were selected using 2 μg/ml puromycin. Individual colonies were expanded and screened for expression following several passages using anti-Myc 1-9E10 monoclonal antibody (MAb).

Cell stimulation and harvesting. Bone marrow-derived mast cell cultures were established from WT, $fes^{K588R/K588R}$ $fer^{D743R/D743R}$ mice, sensitized and stimulated as previously described (67). RBL-2H3 cells and the derivative cell lines described above were seeded onto 100-mm tissue culture dishes at approximately 80% confluence. The following day, cells were starved and sensitized in starvation medium (Dulbecco's modified Eagle's medium supplemented with anti-dinitrophenol [DNP]-IgE [10% vol/vol] conditioned medium from SPE-7 hybridoma) and incubated overnight at 37°C. Cells were then washed with warmed Tyrode's buffer (10 mM HEPES [pH 7.4], 130 mM NaCl, 5 mM KCl, 1.4 mM $CaCl_2$, 1 mM $MgCl_2$, 5.6 mM glucose, 0.1% bovine serum albumin) and resuspended in Tyrode's buffer with or without DNP-conjugated human serum albumin ([HSA] 100 ng/ml; Sigma) and incubated for various times at 37°C. Cells were rinsed with cold phosphate-buffered saline–100 μM sodium orthovanadate and subsequently lysed in KLB medium (10 mM Tris-HCl, pH 7.5, 150 mM NaCl, 1 mM EDTA, 1% [wt/vol] NP-40, 100 μM sodium orthovanadate, 100 μM phenylmethylsulfonyl fluoride, 10 mg/ml aprotinin, 10 mg/ml leupeptin). Soluble cell lysates (SCLs) were prepared following centrifugation at 12,000 × *g* for 5 min at 4°C. Immunoprecipitations (IP) were carried out using 1-9E10 anti-Myc monoclonal hybridoma supernatant (100 μl/IP) for RBL-2H3 cell experiments or HS1 MAb (StressGen; 2 μg/IP) for bone marrow mast cells (BMMCs) and

incubated with GammaBind Sepharose (GE Healthcare Ltd.) overnight at 4°C. Following three washes in KLB medium, immunoblotting (IB) was performed using antiphosphotyrosine MAb (PY99; 1:1,000; Santa Cruz Biotechnology), anti-Myc MAb (1:10), anti-phosphorylated extracellular signal-regulated kinase (anti-pERK) MAb (1:200; Santa Cruz Biotechnology), anti-HS1 MAb (1:1,000; StressGen), anti-FcεRI β-chain MAb (1:1,000), anti-GST rabbit antiserum, and anti-Fes/Fer rabbit serum (1:1,000) (12). Antibody complexes were detected using the following secondary antibody: horseradish peroxidase-conjugated sheep anti-mouse IgG or goat anti-rabbit IgG (both at 1:10,000; GE Healthcare UK, Ltd.). The proteins were visualized by enhanced chemiluminescence (ECL; PerkinElmer Life Sciences, Inc.).

IVK assays. In vitro kinase (IVK) assays were carried out as previously described (67). Briefly, IP were performed with anti-Fes/Fer antiserum (12), washed three times with KLB medium and once in kinase reaction buffer (KRB; 20 mM Tris-HCl [pH 7.5], 10 mM $MnCl_2$, 100 μM sodium orthovanadate). Substrate proteins (GST, GST-HS1 WT, GST-HS1 with the mutation Y388F or Y405F, and a GST-HS1 double mutant lacking both Y388 and Y405) were washed once with KRB, and kinase reactions were performed in KRB supplemented with 100 μM cold ATP and 5 μg of GST fusion proteins as substrates. Reaction mixtures were incubated for 20 min at 30°C, and reactions were terminated by the addition of 2× sodium dodecyl sulfate (SDS) sample buffer (130 mM Tris-HCl [pH 6.8], 20% [vol/vol] glycerol, 2% [vol/vol] SDS, 10% [vol/vol] β-mercaptoethanol, 0.08% [wt/vol] bromophenol blue). Samples were analyzed by IB using PY99 MAb and anti-GST rabbit antiserum and revealed by ECL.

Phosphoinositide binding assays. PIP strip assays were performed as recommended by the manufacturer (Echelon Biosciences, Inc.). Briefly, GST-Fes(1–300) (0.5 μg/ml) was incubated with the PIP strip overnight at 4°C, followed by affinity-purified rabbit anti-GST polyclonal antibody (1:2,000) and horseradish peroxidase-conjugated goat anti-rabbit IgG (1:10,000; GE Healthcare UK Ltd.); proteins were revealed by ECL. Liposome binding assays were performed as previously described (33). Briefly, the GST-Fes(1–459) WT and RK/QQ and RK/EE mutant proteins were subjected to centrifugation at 70,000 rpm for 15 min in a TL100 rotor (Beckman Coulter) to remove protein aggregates. Then, 5 μg of protein was incubated with 100 μg of liposomes [containing phosphatidylcholine/phosphatidylethanolamine (PC/PE; Sigma-Aldrich), with or without phosphatidylserine (PS; Sigma-Aldrich) and $PI(4,5)P_2$ (Echelon Biosciences Inc.)] in binding buffer (0.1 M sucrose, 20 mM HEPES pH 7.4, 100 mM KCl, 1 mM EDTA) for 15 min at 25°C. Following centrifugation at 60,000 rpm for 15 min at 25 C, supernatants and pellets were resuspended in SDS sample buffer and analyzed by Coomassie brilliant blue staining of SDS–11% polyacrylamide gel electrophoresis gels. Liposome tubulation was carried out at room temperature using 0.5 mg/ml PC/PE/PS-based liposomes (as above), with or without $PI(4,5)P_2$(10%), and incubated with 1 μg of recombinant purified F-BAR proteins for 15 min at 25°C prior to plating on a microscope slide and phase-contrast imaging using an Olympus BX51 microscope equipped with a Q Color5 digital camera (100× oil objective with a 1.30 numerical aperture; images were acquired using QCapturePro software).

Degranulation assays. RBL-2H3 cells stably transfected as described above were assayed for degranulation by adapting a previously described assay for histamine release (43) to detection of beta hexosiaminidase release (10). Briefly, cells (10^5) were plated in 24-well plates with triplicate wells for each condition, sensitized with anti-DNP-IgE, and either untreated or treated with DNP-HSA (100 ng/ml) or calcium ionophore A23187 (1 μM; Sigma) in Tyrode's buffer. After 30 min, supernatants were collected, and lysates were prepared for assay of beta hexosiaminidase activity using *p*-nitrophenyl *N*-acetyl-β-D-glucosamine (Sigma) as a substrate. Percent degranulation was calculated as follows: (released activity/total activity) × 100.

Immunofluorescence and live-cell imaging. Myc-Fes^{WT} and Myc-$Fes^{RK/QQ}$ protein localization was detected in IgE-sensitized RBL-2H3 cell lines (with or without DNP-HSA treatment for 20 min), following fixation and permeabilization in 4% paraformaldehyde–0.1% Triton X-100; samples were stained with purified anti-Myc MAb (1:200; Applied Biological Materials Inc.), followed by Alexa633-conjugated goat anti-mouse secondary antibody (1:400; Invitrogen) and fluorescein isothiocyanate-conjugated rat anti-mouse IgE MAb (1:200; Southern Biotechnology). Confocal images were collected using a Leica TCS SP2 multiphoton confocal microscope (equipped with a 100× objective) in the Queen's University Protein Function Discovery facility. For live-cell imaging experiments, COS-7 cells were seeded on gelatin-coated ΔT plates (Bioptics) and transfected with pEGFP-Fes(1–300) or pEGFP-Fes(1–459) (WT or RK/QQ protein) and with a full-length Fes-GFP fusion construct (Fes^{FL}-GFP) that was previously described (71). Transfections were carried out using FuGENE HD according to the manufacturer's instructions (Roche Diagnostics). Cells were rinsed once in Tyrode's buffer and incubated with 10 μg/ml $DiIC_{16}(3)$ fluorescent dye (Invitrogen) for 10 min; this step was followed by live-cell imaging using a Leica TCS SP2 multiphoton confocal microscope (equipped with a 100× objective and heated stage) in the Queen's University Protein Function Discovery facility. Frames were captured every 3 s for 2 min and assembled into time-lapse videos using ImagePro Plus software. Still frames were extracted and are presented individually or as complete time-lapse videos in the supplemental material.

Membrane fractionation. Membrane fractionation was performed as previously described (60). Briefly, RBL-2H3 cell lines grown to confluence in 100-mm plates were serum starved and sensitized with anti-DNP-IgE overnight prior to treatment with or without DNP-HSA (100 ng/ml) for 5 min. Cells were lysed in hypotonic Triton X-100 lysis buffer (20 mM Tris-HCl [pH 7.4], 3 mM $MgCl_2$ 8% sucrose, 0.5% Triton X-100, 5 mM EGTA, supplemented with protease and phosphatase inhibitors), and after clarification at 10,000 × *g*, supernatants were subjected to ultracentrifugation at 60,000 rpm for 2 h. After centrifugation the pellet was designated the membrane fraction, and supernatants comprised the SCL. Pellets were resuspended in SDS sample buffer and boiled for 10 min, and proteins were analyzed by IB with anti-Myc and anti-Lyn MAbs (Santa Cruz Biotechnology).

Modeling of Fes F-BAR domain. Using the known crystal structures of the F-BAR domain (PDB codes 2EFL and 2EFK) (59) as the template, we constructed a three-dimensional model of the human Fes protein using the SWISS-MODEL program (54). A human Fes F-BAR homodimer was generated using the Xtalview program (http://www.sdsc.edu/CCMS/Packages/XTALVIEW/), again based on the F-BAR dimer structure resulting from crystal packing (59). The human $Fes^{RK/EE}$ mutant was also generated, and all models were subjected to further energy minimization. Structural analysis such as charged-surface representation of the human Fes model and its mutant was carried out with the aid of the PyMol graphics program (http://www. pymol.org).

RESULTS

Homology modeling of the Fes F-BAR domain. The N-terminal F-BAR domains of several PCH adaptor proteins were shown to bind and tubulate phosphoinositide-containing liposomes (33, 66). With the solving of F-BAR domain structures from several PCH adaptors (27, 59) and the proposed existence of an N-terminal F-BAR in Fes (3, 26), we prepared a homology model of the Fes F-BAR domain (amino acids 1 to 288), based on the solved structure of FBP17 (59). Despite the relatively low sequence homology between Fes and FBP17 (~15% identity for F-BAR domains), the Fes F-BAR domain model compared very closely with the structure of FBP17 as both a monomer (data not shown) and a dimer (Fig. 1A). The curvature of the Fes F-BAR dimer is conserved, as is the alignment with the critical curvature-inducing P210 residue within the α4 helix (Fig. 1D). A comparison of the concave phospholipid-binding surface of the Fes F-BAR domain with that of FBP17 (Fig. 1B) shows that although a key pair of basic residues (R113/K114) is conserved in Fes, the patches of basic residues on the concave surface appear less contiguous in the Fes F-BAR domain than in that of FBP17. However, the Fes F-BAR domain does have an extensive cluster of basic residues at the tips of the F-BAR domain (Fig. 1B). A model of the Fes F-BAR domain with glutamates for R113/K114 reveals a dramatic reduction in basic residues in the middle phospholipid binding pocket, without affecting the basic cluster (Fig. 1C). This Fes/Fer-specific basic cluster is created by an extended region of basic residues occurring at every second position near the beginning of α4 (amino acids 163 to 174) compared to FBP17 and CIP4 (Fig. 1D). These differences in the charged surfaces within the putative phosphoinositide-binding face of the Fes F-BAR domain may confer novel lipid-binding or localization properties to Fes/Fer PTKs. It is also worth noting that outside of the conserved R113/K114 residues, Fes/Fer

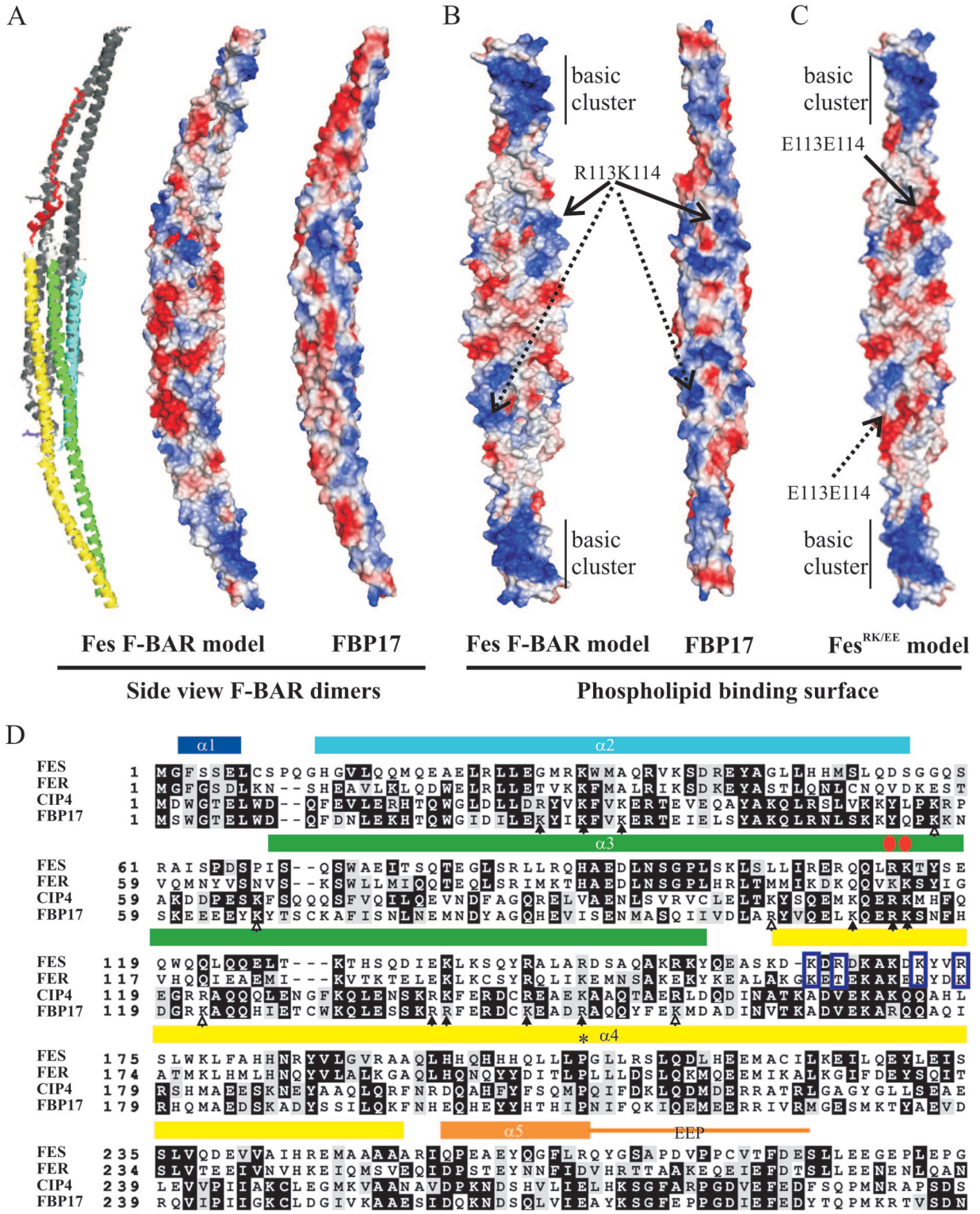

FIG. 1. Homology modeling of the Fes F-BAR domain. The F-BAR domain of human Fes was modeled on the FBP17 F-BAR domain crystal structure (PDB codes 2EFL and 2EFK) (66) as described in Materials and Methods. (A) Fes F-BAR homodimer was generated with the Xtalview program and analyzed in PyMol, and both ribbon and charged-surface representations are shown. Basic residues are shown in blue, and acidic residues are in red for the Fes model and FBP17 structure. (B) The predicted phospholipid binding (concave) faces of the F-BAR domains are shown. The relative positions of conserved residues R113/K114 are indicated by solid and dashed arrows within the Fes F-BAR domain dimer. An more extended patch of basic residues (basic cluster) in Fes compared to FBP17 is indicated near each end of the dimer. (C) A homology model of the $Fes^{RK/EE}$ mutant F-BAR domain showing the predicted loss of the central basic residues on the phospholipid-binding face. (D) Multiple sequence alignment of F-BAR domains from human Fes, Fer, CIP4 and FBP17 (from the Baylor College of Medicine Search Launcher using pattern-induced [local] multiple alignment; http://searchlauncher.bcm.tmc.edu/multi-align/Options/pima.html) displayed using the Boxshade

retain few of the additional basic residues recently shown to directly contact phospholipids within curved membranes (Fig. 1D) and for binding flat membrane sheets (Fig. 1D) (16).

Phosphoinositide binding properties of the Fes F-BAR domain. To determine the potential ability of the Fes F-BAR domain to bind phospholipids, we prepared GST-Fes fusion proteins encoding the F-BAR domain [Fes(1–300)] or an extended construct including F-BAR and the CC2/3 domains, Fes(1–459) (Fig. 2A). Mutations to the conserved R113/K114 residues were conferred to either remove (RK/QQ) or reverse (RK/EE) the basic charges. To survey for potential ligands of the Fes F-BAR domain, PIP strips were probed with either recombinant purified GST, GST-Fes(1–300), or GST-Fes(1–459), and bound proteins were revealed by IB with anti-GST. While no signals were obtained with GST (data not shown), the Fes F-BAR domain (residues 1 to 300) bound all phosphoinositides but not other charged phospholipids (e.g., PS and sphingosine-1-phosphate). Addition of CC2/3 domains to the F-BAR [Fes(1 to 459)] modulated the phospholipid-binding profile to include detectable binding of PI and PS (Fig. 2B). These results provide evidence that the Fes N-terminal domain does bind phospholipids and suggest potential cooperative interactions beyond the F-BAR domain sequences that correspond to the solved structures (27, 59). Other F-BAR domains have been shown to cause liposome tubulation in vitro. To test whether this activity was conserved in Fes, we prepared PC/PE/PS-based liposomes that were supplemented with or without $PI(4,5)P_2$ and incubated them with Fes(1-300) or Fes(1-459) proteins. In the absence of $PI(4,5)P_2$, liposomes were round, whereas we observed extended tubular extensions of $PI(4,5)P_2$-containing liposomes with both Fes F-BAR constructs (Fig. 2C). To measure phospholipid binding and the effects of mutations within the Fes F-BAR domain, we performed liposome sedimentation assays using PC/PE-based liposomes supplemented with or without PS and $PI(4,5)P_2$(as described in reference 33). We compared binding of Fes(1-300) and Fes(1-459) proteins and found that these proteins were highly enriched in the pellet fraction of $PI(4,5)P_2$-containing liposomes compared to control liposomes (Fig. 2D). However, the RK/QQ and RK/EE mutations within the Fes(1-459) protein caused a ~50% decrease in binding of $PI(4,5)P_2$-containing liposomes compared to WT Fes(1-459) (Fig. 2D).

The Fes F-BAR domain localizes to tubular structures within the cytoplasm and at the cell periphery. Since overexpression of the F-BAR domains from PCH adaptor proteins (e.g., FBP17) can cause extensive tubulation of membranes (33, 66), we tested whether this is a potential activity of the Fes F-BAR domain. We performed live-cell imaging of COS-7 cells expressing GFP fused to Fes^{FL} or to Fes(1–459) and Fes(1–300) (either WT or harboring the RK/QQ mutation). Prior to microscopy, membranes were counterstained using $DiIC_{16}(3)$ (Fig. 3). Similar to previous studies on fixed cells, Fes^{FL} localization was highest in the perinuclear region, consistent with the *trans*-Golgi apparatus (as previously reported [71]), and along large tubules that likely correspond to microtubules (as previously reported in reference 37). Interestingly, some $DiIC_{16}(3)$-positive vesicles colocalized with and appeared to traffic along Fes^{FL}-positive tubules (Fig. 3; see time-lapse video in the supplemental material). To examine localization conferred by the Fes N-terminal domain and the contributions of its phosphoinositide binding, we compared subcellular localization of the Fes(1–459) WT and RK/QQ proteins. Although less prominent than Fes^{FL}, $Fes(1–459)^{WT}$ displayed some tubular staining that colocalized with $DiIC_{16}(3)$-positive vesicles within the cytoplasm and at the cell periphery (Fig. 3). In contrast, the $Fes(1–459)^{RK/QQ}$ mutant displayed more uniform localization and no obvious colocalization with $DiIC_{16}(3)$-positive membranes. Interestingly, $Fes(1–300)^{WT}$ was found to localize to dynamic tubules formed near the cell periphery that were colocalized with $DiIC_{16}(3)$-positive membranes (Fig. 3, bottom left panel; see time-lapse video in the supplemental material). Mutation of the phosphoinositide binding site caused a more diffuse cytoplasmic localization pattern of $Fes(1–300)^{RK/QQ}$ compared to that of $Fes(1–300)^{WT}$. Taken together, these results suggest that phosphoinositide binding via the F-BAR domain of Fes can alter its subcellular localization relative to membrane compartments in live cells.

The F-BAR domain of Fes is required for FcεRI-evoked phosphorylation in mast cells. Our previous studies of Fes and Fer PTK activation downstream of FcεRI in mast cells provided evidence for tyrosine phosphorylation (pY) of Fes/Fer by an upstream PTK (55). One candidate PTK we identified in this pathway is Lyn (67), an Src family PTK that is constitutively localized to the plasma membrane. Hence, membrane localization of Fes via the F-BAR domain may allow for Fes activation by FcεRI-associated Lyn PTK. RBL-2H3 cells and derivates stably expressing Myc-Fes^{WT}, Myc-Fes^{K588R} (kinase-dead), or Myc-$Fes^{RK/QQ}$ were generated to determine the role of the F-BAR domain in its activation via the FcεRI pathway. Following sensitization of the cells with anti-DNP-IgE and stimulation with antigen (DNP-HSA) for various times, we observed inducible pY of Myc-Fes^{WT} (Fig. 4A, upper panel). In contrast, no detectable pY of Myc-$Fes^{RK/QQ}$ was observed. This is despite similar recovery of Myc-Fes^{WT} or Myc-$Fes^{RK/QQ}$ in the immunoprecipitates (Fig. 4A, middle panel). To confirm that FcεRI-evoked signaling was indeed initiated in all cell lines, a pERK mitogen-activated protein kinase IB of SCLs revealed similar FcεRI-evoked pERK levels and kinetics in each cell line (Fig. 4A, bottom panel). To confirm that the F-BAR mutation did not have unpredicted effects on Fes PTK activity, IVK assays were performed (Fig. 4B). No significant differences were observed in either autophosphorylation (pY-Fes) or substrate phosphorylation between WT and RK/QQ Fes proteins (Fig. 4B) (the ratio of pY Fes to total Fes was deter-

server (http://www.ch.embnet.org/software/BOX_form.html). Amino acid numbers are shown on the left, and aligning, identical residues are shaded in black, while conserved residues are shaded gray. The positions of α1 to α5 and the F-BAR extended peptide (EEP) are shown above the residues, based on the structure of FBP17 (59), and are color matched to the ribbon model shown in panel A. Red circles indicate the positions of R113/K114, an asterisk indicates a conserved proline involved in generating F-BAR domain curvature, and blue boxes indicate residues in Fes/Fer PTKs that contribute to the extended basic cluster at the ends of the dimer in panel B. Closed arrows indicate residues in CIP4 shown by Frost et al. to contact lipids of curved membranes, and open arrows indicate residues in CIP4 implicated in binding flat membrane sheets (16).

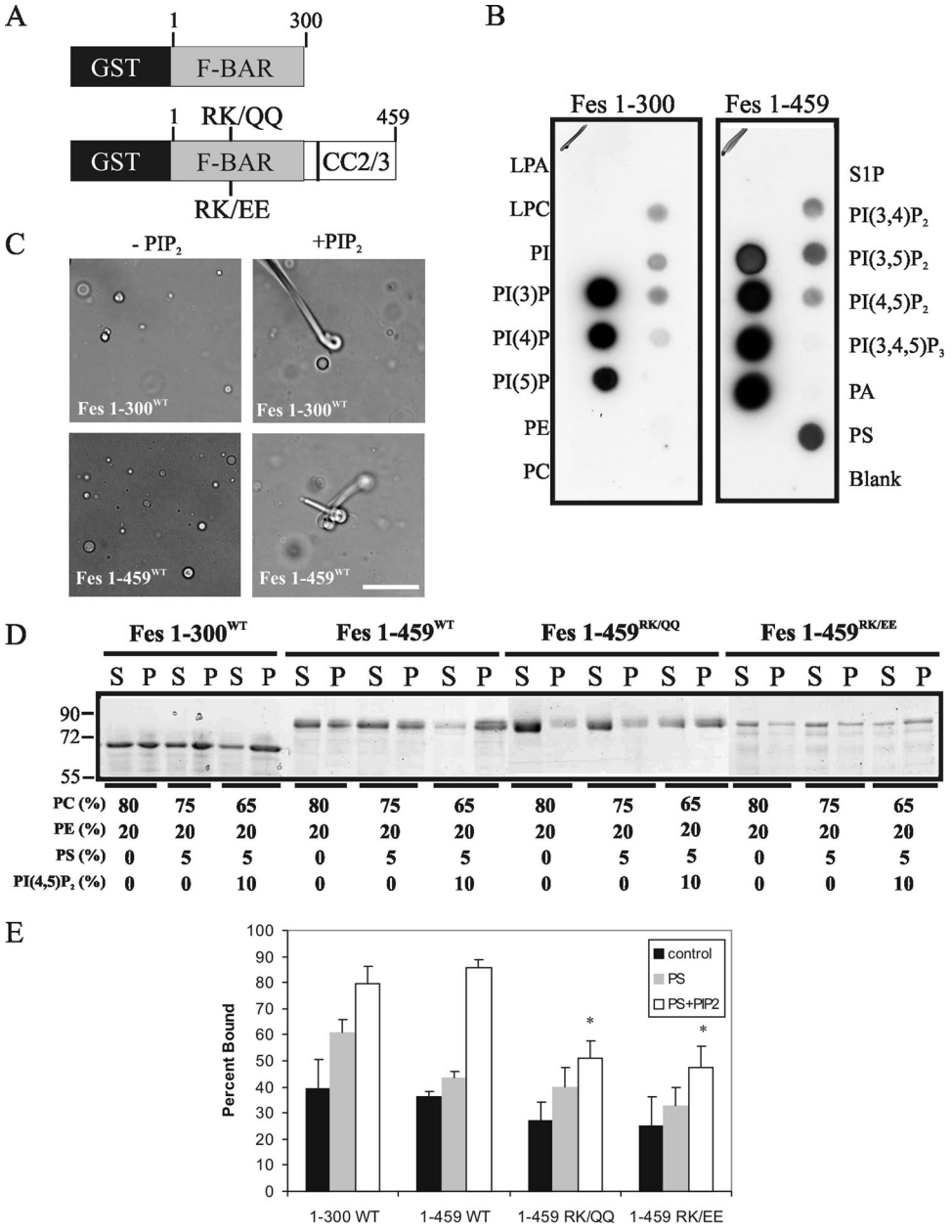

FIG. 2. Requirement of conserved basic residues for phospholipid binding via the Fes F-BAR domain. (A) Schematic representation of the GST-Fes(1–300) and GST-Fes(1–459) fusion proteins and the positions of RK/QQ and RK/EE mutations. (B) Phospholipid binding screen of the GST-Fes(1–300) and GST-Fes(1–459) proteins with phospholipids arrayed on a filter (PIP Strip; Echelon Bioscience, Inc.). Relative positions of lipid spots are as follows: LPA, lysophosphatidic acid; LPC, lysophosphatidylcholine PI, phosphatidylinositide; PI(3)P, phosphatidylinositol-3-phosphate; PI(4)P, phosphatidylinositol-4-phosphate; PI(5)P, phosphatidylinositol-5-phosphate; S1P, sphingosine-1-phosphate; $PI(3,4)P_2$, phosphatidylinositol-3,4-bisphosphate; $PI(3,5)P_2$, phosphatidylinositol-3,5-bisphosphate; $PI(4,5)P_2$, phosphatidylinositol-4,5-bisphosphate; $PI(3,4,5)P_3$, phosphatidylinositol-3,4,5-trisphosphate; PA, phosphatidic acid. A blank was included. (C) Liposome tubulation assays were carried out with PE/PC/PS-based liposomes, alone or supplemented with $PI(4,5)P_2$, that were incubated with purified Fes(1–300) and Fes(1–459) proteins, as described in Materials and Methods. Representative phase-contrast images are shown. Scale bar, 10 μm. (D) Liposome sedimentation assays using liposomes composed of the indicated combinations of PC, PE, PS, and $PI(4,5)P_2$, incubated with purified GST-Fes(1–300), GST-Fes(1–459)^{WT}, GST-Fes(1–459)$^{RK/QQ}$, or GST-Fes(1–459)$^{RK/EE}$ protein. Following liposome sedimentation the amount of GST fusion proteins in supernatant (S) and pellet (P) were analyzed by SDS-polyacrylamide gel electrophoresis, followed by Coomassie brilliant blue staining. (E) The results from four to six independent liposome sedimentation assays were quantified by densitometry (graph depicts mean ± standard error of the mean). Asterisks indicate a significant difference ($P < 0.05$ compared to GST-Fes(1–459)^{WT} by t test).

mined by densitometry[relative Fes pY]; PECAM-1(CT) was previously identified as an Fer/Fes substrate) (67). Further evidence that effects on kinase activity are unlikely to account for the defects in IgE/DNP-induced pY of Myc-Fes$^{RK/QQ}$ is the observed IgE/DNP-induced phosphorylation of a Myc-tagged kinase-dead Fes (Fes^{K588R}; classical ATP-binding fold mutation) in this system (Fig. 4C). These results are consistent with our previous studies that show that Fer/Fes are substrates for an upstream

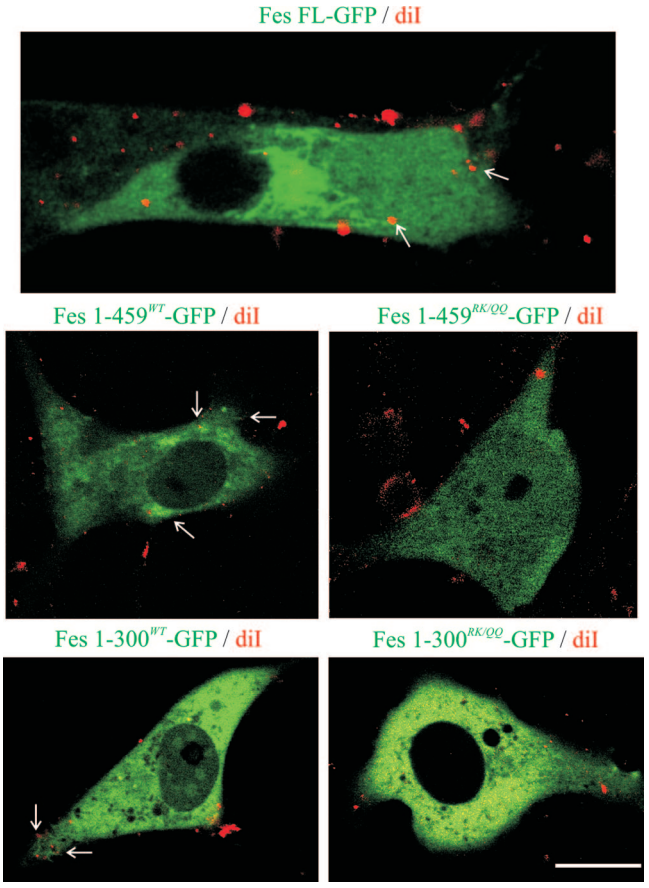

FIG. 3. The Fes F-BAR domain contributes to tubular localization of Fes in live cells. Live-cell imaging of COS-7 cells transfected with GST-Fes(1–459)^{WT}, GST-Fes(1–459)$^{RK/QQ}$, and GST-Fes^{FL} were incubated with $DiIC_{16}(3)$ (dil) and imaged by confocal microscopy as described in Materials and Methods. Representative confocal microscopy images are shown with overlays of GFP (green) and $DiIC_{16}(3)$-positive membranes (red). Arrows indicate sites of membrane tubulation. Scale bar, 20 μm. For time-lapse videos showing the dynamic patterns of Fes localization, see the supplemental material.

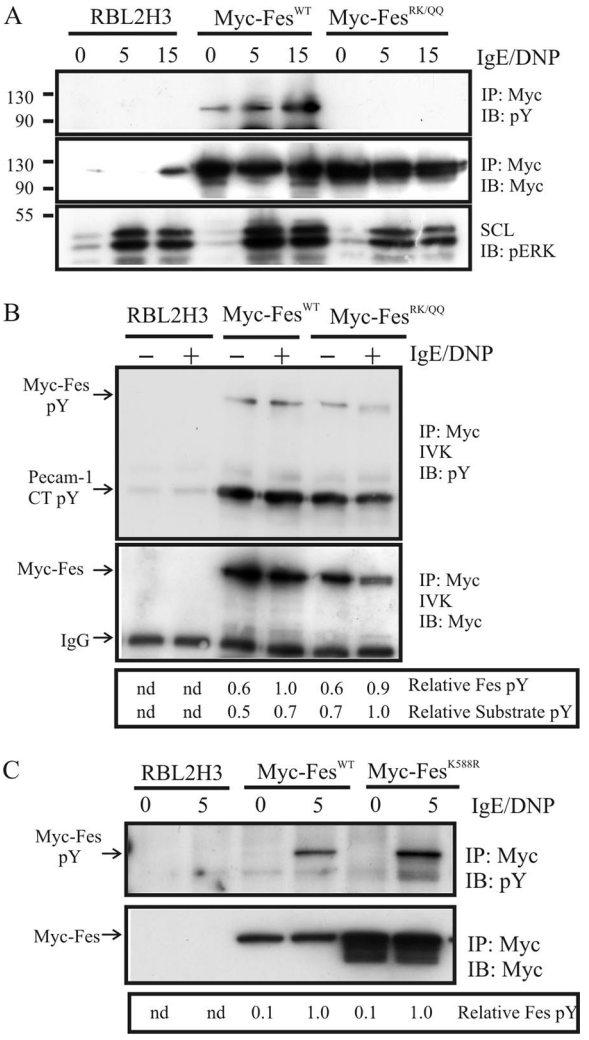

FIG. 4. The F-BAR domain of Fes is required for FcεRI-evoked Fes phosphorylation in mast cells. (A) RBL-2H3 cells and derivatives stably expressing Fes^{FL}, Myc-Fes^{WT}, or Myc-Fes$^{RK/QQ}$ were starved and sensitized with anti-DNP-IgE and stimulated for various times (min) with DNP-HSA (100 ng/ml). SCLs were prepared and subjected to either IB with anti-pERK or IP with anti-Myc antibody, followed by IB with anti-pY. The blot was stripped and reprobed with anti-Myc antibody. (B) IVK assays were performed using the same cell lines as above. The relative positions of Myc-Fes autophosphorylation (pY) and substrate phosphorylation (PECAM-1 CT pY) (67) are indicated on the left. The blot was reprobed with anti-Myc to document the relative amounts of Myc-Fes^{WT} and Myc-Fes$^{RK/QQ}$ in the IVK assay. The position of the IgG heavy chain is indicated on the left. Relative Fes pY and substrate pY were quantified by densitometry. (C) RBL-2H3 cells and derivatives stably expressing Myc-Fes^{WT} or the kinase-dead mutant Myc-Fes^{K588R} were starved and sensitized with anti-DNP-IgE and stimulated for 5 min with DNP-HSA. Lysates were subjected to IP with anti-Myc and to IB with anti-pY and anti-Myc. The positions of the Myc-Fes proteins are indicated on the left. Relative Fes pY was determined by densitometry. nd, not detected.

PTK (e.g., Lyn) (55, 67). This suggests that phosphoinositide binding via the F-BAR domain of Fes may contribute to its localization to FcεRI/Lyn complexes in the plasma membrane.

Role of Fes F-BAR domain in regulating degranulation and Fes localization in mast cells. To gain further insights into the potential role of the F-BAR domain of Fes for regulating FcεRI aggregation-induced responses of mast cells, we performed degranulation assays on the vector-, Myc-Fes^{WT}-, and Myc-Fes$^{RK/QQ}$-transfected RBL-2H3 cell line. Compared to vector-transfected cells, overexpression of Myc-Fes^{WT} led to increased IgE/DNP-triggered degranulation (Fig. 5A). It is worth noting that no differences were observed with IgE or calcium ionophore (A23187) treatment. Interestingly, IgE/DNP-triggered degranulation was reduced in Myc-Fes$^{RK/QQ}$-expressing RBL-2H3 cells compared to vector- or Myc-Fes^{WT}-transfected cells. This was not due to defects in granule contents as these cells were found to degranulate very efficiently in response to ionophore. The defects in FcεRI-induced degranulation were not due to loss of surface FcεRI, as demonstrated by flow cytometry (Fig. 5B). Taken together, these results suggest that the F-BAR domain of Fes is required for Fes to regulate degranulation of mast cells.

To gain further insights into the potential role of the F-BAR domain for Fes localization in mast cells, we performed immunofluorescence staining of Myc-Fes and FcεRI in anti-DNP-IgE-sensitized stable transfectants of RBL-2H3

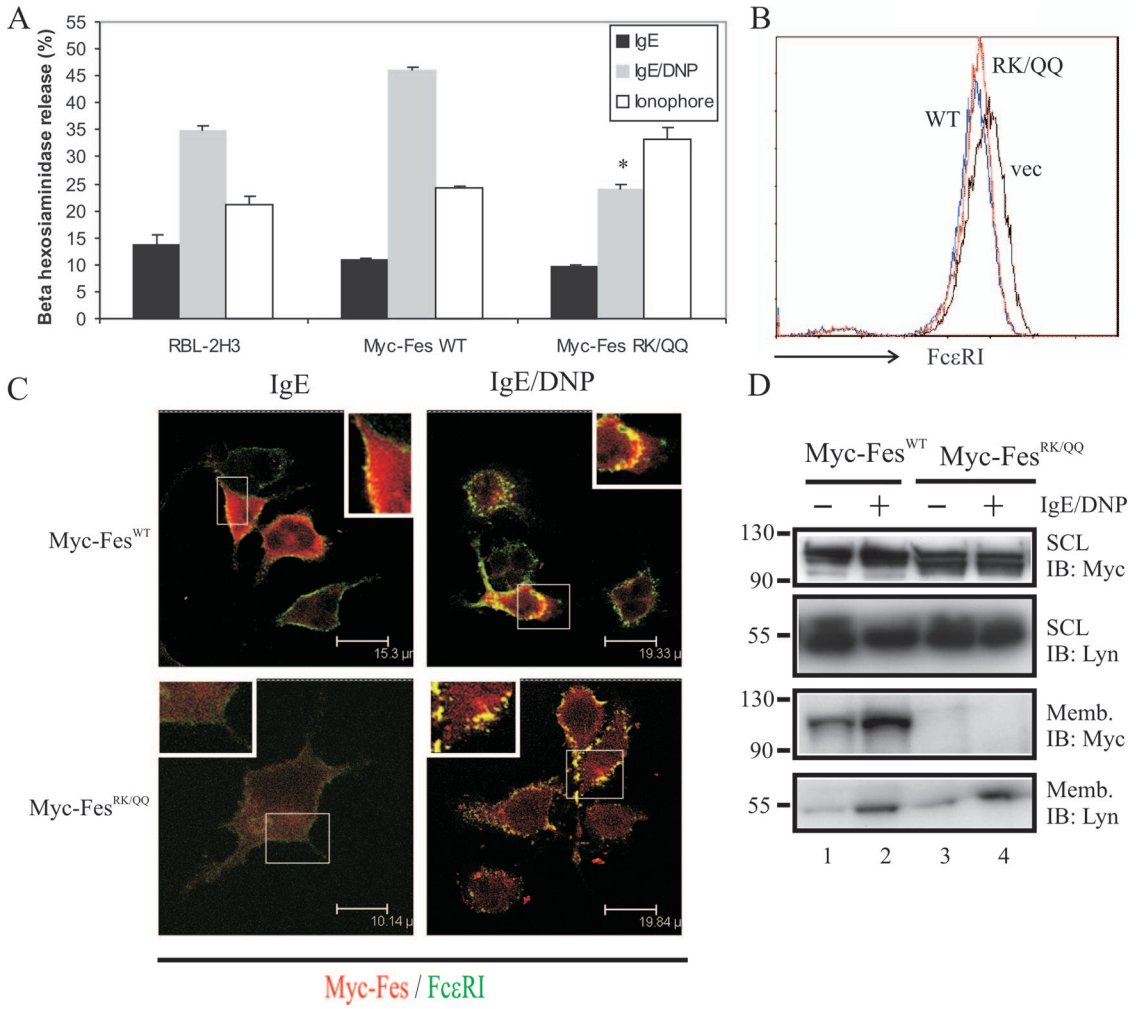

FIG. 5. Contributions of Fes F-BAR to regulation of degranulation and localization in RBL-2H3 mast cells. (A) Vector-transfected RBL-2H3 cells and Myc-Fes^{WT}- or Myc-Fes$^{RK/QQ}$-expressing cells were sensitized with anti-DNP-IgE and assayed for degranulation in response to antigen or calcium ionophore, as described in Materials and Methods. (B) Surface expression of FcεRI was determined for RBL-2H3 cells stably transfected with MSCV vector (vec), Myc-Fes^{WT}, and Myc-Fes$^{RK/QQ}$. (C) Localization of Myc-Fes^{WT} and Myc-Fes$^{RK/QQ}$ was analyzed in IgE-sensitized cells (with or without DNP-HSA treatment for 20 min) by immunofluorescence, as described in Materials and Methods. Representative confocal images showing Myc-Fes staining in red and FcεRI in green are shown (yellow indicates colocalization). Scale bars are shown in the lower right of each panel. (D) Membrane fractions were prepared from Myc-Fes^{WT}- and Myc-Fes$^{RK/QQ}$-transfected RBL-2H3 cells as described in Materials and Methods. SCLs and membrane fractions (Memb) were subjected to IB with Myc and Lyn antibodies. Positions of molecular mass markers are indicated on the left.

cells, treated with or without antigen. Confocal microscopy images revealed exclusively plasma membrane localization of FcεRI for IgE-treated cells and extensive FcεRI clustering and internalization in both cell lines following antigen challenge for 20 min (Fig. 5C). Interestingly, Myc-Fes^{WT} localized in a punctate pattern within the cytoplasm but also colocalized with FcεRI at the plasma membrane (Fig. 5C). We also detected colocalization of Myc-Fes^{WT} in the perinuclear region with internalized FcεRI in IgE/DNP-treated cells (Fig. 5C, upper right panel). The F-BAR domain likely contributes to the plasma membrane localization since less colocalization of Myc-Fes$^{RK/QQ}$ was observed with FcεRI at the plasma membrane in resting mast cells (Fig. 5C, lower left panel). However, upon antigen-induced FcεRI internalization, some colocalization of Myc-Fes$^{RK/QQ}$ with FcεRI was detected (Fig. 5C, lower right panel). To address the contributions of the F-BAR domain to membrane localization, we performed membrane fractionation on Myc-Fes^{WT}- and Myc-Fes$^{RK/QQ}$-transfected RBL-2H3 cells. Similar amounts of Myc-Fes proteins were expressed in these cells, as detected in the SCLs (Fig. 5D). However, Myc-Fes^{WT} and Lyn were readily detected in the membrane fraction, whereas Myc-Fes$^{RK/QQ}$ was only weakly detected (Fig. 5D, lower panels). These results suggest that the F-BAR domain plays a key role in localization to membranes prior to FcεRI activation but do not rule out other interactions possibly mediated by the SH2 domain following FcεRI phosphorylation and downstream signaling.

Fes SH2 domain interactions with FcεRI and HS1 in mast cells. We next wished to address how the Fes SH2 domain may contribute to its coupling to the activated FcεRI or Fes substrates in mast cells. The consensus sequence for the Fes SH2

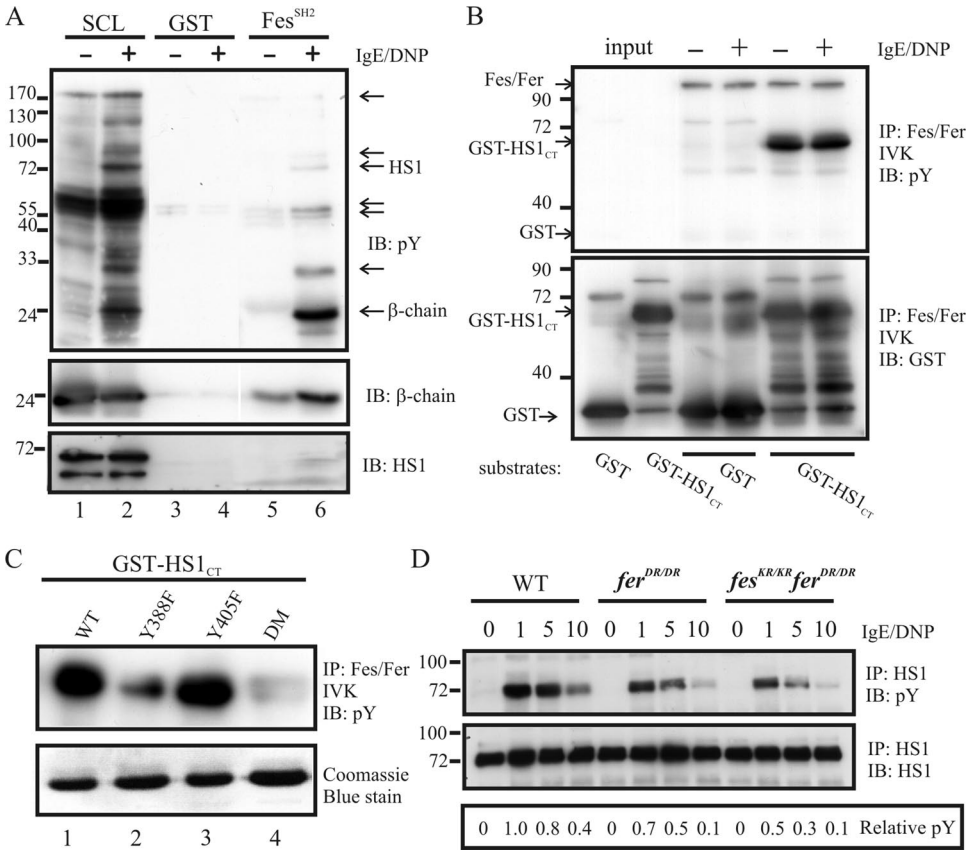

FIG. 6. Fes SH2 interactions with FcεRI and its putative substrate HS1 in mast cells. (A) BMMCs were serum starved, sensitized with anti-DNP-IgE, and treated with or without DNP-HSA for 5 min. Lysates were prepared and incubated with purified GST, or GST-Fes^{SH2} fusion protein bound to glutathione-Sepharose beads. Following extensive washing, IB with anti-pY was performed. Relative molecular mass markers are shown on the left, and arrows on the right indicate Fes^{SH2}-bound pY-containing proteins. IB performed with anti-β chain and anti-HS1 antibodies on duplicate membranes identified these proteins as potential Fes^{SH2} ligands. (B) IVK assays were performed on Fes/Fer IPs (using a cross-reactive antiserum described previously) (12) from lysates prepared from RBL-2H3 cells sensitized with anti-DNP-IgE and treated with or without DNP-HSA for 2 min. Purified GST and GST-HS1$_{CT}$ were used as substrates in either a mock reaction (input) or Fes/Fer IPs. IVK samples were analyzed by IB with anti-pY and anti-GST antibodies. The positions of autophosphorylated Fes/Fer and of GST proteins are indicated by arrows on the left. Substrates added to each reaction mixture are shown at the bottom. (C) Similar IVK assays were performed for GST-HS1$_{CT}$ fusion proteins harboring the mutations Y388F or Y405F or a double mutant encompassing both mutations (DM). IVK assays were analyzed by IB with anti-pY (upper panel), and substrate amounts are shown by Coomassie brilliant blue staining (lower panel). (D) BMMCs from WT, *fer*$^{D743R/D743R}$ (*fer*$^{DR/DR}$), and *fes*$^{K588R/K588R}$ *fer*$^{D743R/D743R}$ (*fes*$^{KR/KR}$ *fer*$^{DR/DR}$) mice were generated, starved of interleukin-3, and sensitized with anti-DNP-IgE. Following treatment with DNP-HSA for the indicated times (min), lysates were prepared and subjected to IP with anti-HS1 and to IB with either anti-pY or anti-HS1. The relative HS1 pY (ratio of pY HS1/total HS1) was determined by densitometry, and values are relative to WT cells treated for 1 min.

domain was originally defined as pYEX(V/I) (62) and more recently defined as pY(E/y/i/m/d)(N/e/m/l)(V/Y/E/l), with the most highly preferred amino acids shown in uppercase letters (30). To test for interacting partners of the Fes SH2 domain (Fes^{SH2}) in mast cells, lysates from IgE-sensitized BMMCs (treated with or without DNP-HSA) were incubated with GST or a GST-Fes^{SH2} fusion protein bound to beads. IB with anti-pY revealed several pY-containing proteins recovered with Fes^{SH2} (Fig. 6A, lanes 5 and 6). Very few proteins were detected in the control GST pull-down samples (lanes 3 and 4). By taking a candidate approach, we identified the FcεRI β chain and HS1 as the 24- and 72-kDa proteins, respectively. Thus, the Fes^{SH2}-mediated interaction with FcεRI may contribute to its recruitment and/or localization with the activated receptor.

Since cortactin is a substrate of Fer PTK in fibroblasts responding to platelet-derived growth factor or reactive oxygen species (11, 53), we investigated whether HS1 is also a potential direct substrate of Fes or Fer PTK. IVK assays were performed on Fes/Fer IPs from RBL-2H3 mast cells (with or without IgE or antigen) using either GST or GST-HS1$_{CT}$ as substrates (Fig. 6B). Strong pY of GST-HS1$_{CT}$ was evident, with no detectable pY in mock reactions (input) without Fes/Fer PTKs. No GST pY was detected. We next addressed the potential sites of HS1 pY by mutating two previously identified phosphorylation sites (6). Although the Y388F mutant had the most dramatic effect on Fes/Fer PTK-induced phosphorylation of the single mutants, a double mutant (Y388F/Y405F) was required to eliminate detectable HS1 pY (Fig. 6C). Similar amounts of each substrate were compared in these IVK assays, as shown by Coomassie blue staining (Fig. 6C, bottom panel).

Although HS1 was previously shown to undergo FcεRI-

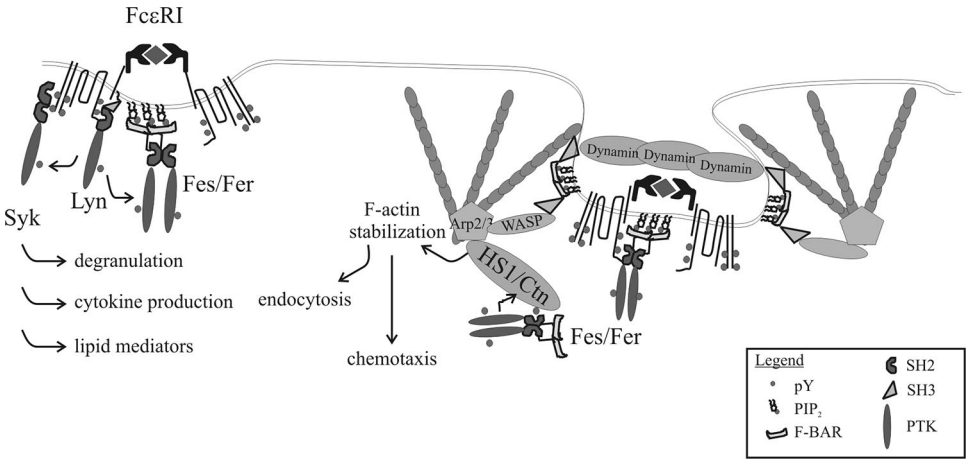

FIG. 7. A potential model for contributions of F-BAR-containing adaptor proteins and PTKs in regulating FcεRI signaling during internalization. FcεRI-evoked activation of Fes and Fer PTKs involves the actions of an upstream PTK (e.g., Lyn), which is facilitated by F-BAR domain-mediated membrane localization. F-BAR-containing adaptor proteins are known to induce membrane invagination and dynamic actin assembly via SH3-mediated recruitment of WASP and dynamin. We hypothesize that Fes and Fer PTK recruitment of HS1 by Fes^{SH2} and its subsequent phosphorylation contribute stabilization of branched F-actin that promotes endocytosis and chemotaxis of mast cells.

induced pY in mast cells (17), the candidate PTKs and the role of HS1 in mast cells remain unclear. BMMCs were generated from WT, $fer^{D743R/D743R}$ (no Fer activity) and $fes^{K588R/K588R}$ $fer^{D743R/D743R}$ (no Fes or Fer activities) mice (55). Following sensitization with anti-DNP-IgE and challenge with DNP-HSA for various times, lysates were prepared and subjected to IP with anti-HS1. IB with anti-pY revealed a slight decrease (30%) in HS1 pY in Fer-deficient BMMCs and a more profound decrease (>50%) in total HS1 pY in Fes/Fer kinase activity-deficient BMMCs (Fig. 6D). These results suggest that HS1 is a substrate of Fes/Fer PTKs in vitro and in vivo.

DISCUSSION

In this study, we present new insights into how Fes PTK utilizes its F-BAR and SH2 domains for its coupling to the FcεRI pathway in mast cells. Several recent advances have helped define F-BAR domains as novel phosphoinositide-binding modules with membrane tubulation activity (33, 66). Solved structures of F-BAR domains reveal a largely α-helical bundle structure that forms a gently curved dimer with a highly basic charged phospholipid binding face (27, 59). A conserved proline residue (P210 in FBP17) induces the curvature within α4 that helps generate the concave shape of this domain. This proline residue in Fes and Fer PTKs likely denotes the C-terminal boundary of what was previously thought to be a CC domain (CC1) in Fer and Fes PTKs (19). The CC1 and CC2 domains were previously implicated in oligomerization of Fes and Fer (7, 12, 36). In the case of Fes, deletion or proline-insertion mutagenesis of CC1 resulted in elevated Fes PTK activity and an increased ability to promote malignant transformation of fibroblasts and myeloid differentiation (7, 8). Earlier studies pointed to an important function for the v-Fps N-terminal domain for membrane localization and transformation (5, 63). It will now be important to characterize these mutations with respect to their potential effects on phosphoinositide binding and localization of Fes. In this study, we show that a mutation within the F-BAR domain (RK/QQ) blocks Fes PTK activation downstream of FcεRI in RBL-2H3 mast cells and provide evidence for an altered localization pattern of the mutant protein. We hypothesize that this mutation effectively uncouples Fes from the pathway by reducing its localization to FcεRI/Lyn complexes in the plasma membrane (Fig. 7). In the future, it will be very interesting to visualize localization of phosphorylated Fes in activated mast cells. Previous studies have reported localization of Fes to microtubules (64) and evidence for Src family kinases in Fes activation (37). Mast cell activation by FcεRI causes rapid formation of microtubules near the cell periphery that function in translocation of granules to the plasma membrane during degranulation (45). Interestingly, we show in this study that Fes overexpression modulates degranulation in mast cells, and this requires the F-BAR domain. Potential Fes substrates that have been implicated in regulating degranulation include the immunoreceptor tyrosine-based inhibitory motif-containing protein PECAM-1 (67) and *N*-ethylmaleimide-sensitive factor, a key regulator of vesicle fusion (32). Future studies will be needed to investigate whether the Fes F-BAR domain is required for localization and phosphorylation of *N*-ethylmaleimide-sensitive factor or PECAM-1 in mast cells.

In this study, we identify HS1 as both an SH2 domain ligand of Fes and as a direct substrate of Fes and Fer PTKs in mast cells. HS1 contains several sites of tyrosine phosphorylation within its C-terminal domain, including Y388 and Y405, both of which fit the consensus motifs for SH2 binding (388-YEDV-391 and 405-YEDV-408 in mouse HS1) and substrate phosphorylation (61, 62). Although overall tyrosine phosphorylation of HS1 is not completely abrogated in BMMCs devoid of Fes/Fer kinase activities, the remaining tyrosine phosphorylations are likely due to Lyn and/or Syk PTK-mediated priming on other residues (6, 23). Our results showing that HS1 is both an SH2 binding partner and substrate are consistent with a recent paper describing the crystal structure of the SH2-PTK domains of Fes (14). In this study, positive interactions between the SH2 and PTK domains within Fes were mapped, and

interaction with pY-containing SH2 ligand peptides were found to increase catalytic activity from the kinase domain of Fes. Tyrosine phosphorylation of HS1 correlates with its translocation to the plasma membrane following platelet activation (6) and to the immune synapse in T cells upon contact with antigen-presenting cells (18). Formation of the immune synapse requires HS1 phosphorylation, which promotes Vav1 recruitment and filamentous actin (F-actin) polymerization. Vav1 is a guanine nucleotide exchange factor that activates the Cdc42 and Rac GTPases that promote F-actin branching through effectors such as WASP (29). HS1 associates with Arp2/Arp3 and F-actin and synergizes with WASP family proteins to stabilize branched F-actin networks (24, 68). Tyrosine phosphorylation of HS1 could regulate these activities since tyrosine phosphorylation of cortactin promotes branch point stabilization by facilitating the displacement of WASP (38). Presumably, the same model applies to HS1. Future studies will investigate whether hypophosphorylation of HS1 in Fer-deficient BMMCs contributes to their defective chemotaxis (10) and whether this is exacerbated in BMMCs lacking both Fes and Fer PTKs.

Following activation of mast cells by IgE or antigen, FcεRI is rapidly internalized, and this involves Rab5 GTPase, a key regulator of endocytosis (70), and its activation by RabGEF1/Rabex-5 (34). Interestingly, FcεRI aggregation leads to increased expression of RabGEF1, which is predicted to increase subsequent endocytosis of both FcεRI and c-Kit receptors (35). This negative feedback mechanism is physiologically relevant since RabGEF1$^{-/-}$ mice develop severe skin inflammation and have elevated numbers of dermal mast cells (65). Several F-BAR- and SH3-containing adaptor proteins have been shown to promote receptor-mediated endocytosis (33, 66). The proposed model to explain this activity (Fig. 7) involves localized membrane curvature induced by F-BAR domains, together with SH3 domain-mediated recruitment of regulators of actin assembly and endocytosis (e.g., N-WASP and dynamin) (9). Interestingly, previous studies have implicated both v-Fps in promoting internalization of platelet-derived growth factor receptor in fibroblasts (2) and Fes^{WT} PTK in promoting Toll-Like receptor 4 internalization in macrophages (48). Based on our results showing colocalization of Fes with both surface and internalized FcεRI (Fig. 5C), it will be interesting to investigate whether Fes/Fer PTKs also participate in regulating actin assembly during receptor endocytosis of c-Kit or FcεRI on mast cells (Fig. 7). Phosphoinositide binding via the Fes/Fer PTKs may allow for colocalization with PCH adaptors at sites of membrane invagination. PCH adaptor proteins can promote initial F-actin branching and actin assembly via WASP/N-WASP-dependent recruitment of Arp2/Arp3. For stabilization of F-actin branching, HS1 (or cortactin in nonhematopoietic cells) is recruited and interacts with Fes or Fer PTKs via their SH2 domains. Phosphorylation of HS1 by Fes or Fer PTKs may then displace WASP and promote stabilization of F-actin branches that drive invagination of the plasma membrane and endosome closure by dynamin. Interestingly, WASP-deficient mast cells display defects in F-actin reorganization, degranulation, and cytokine production upon FcεRI aggregation (49). Future work will therefore focus on whether Fes and Fer PTKs are redundant in these proposed roles and whether loss of HS1 protein or phosphorylation sites has the predicted effects on FcεRI internalization and signaling.

ACKNOWLEDGMENTS

We gratefully acknowledge the gifts of valuable reagents and advice from Peter Greer and Toshiaki Kawakami. We thank Jeff Mewburn for his help with confocal microscopy and Chris Nicol for use of his fluorescence microscope.

This work is supported by a CIHR New Investigator award (A.W.B.C.) and an operating grant from CIHR to A.W.B.C. (MOP 82882).

REFERENCES

1. **Abramson, J., and I. Pecht.** 2007. Regulation of the mast cell response to the type 1 Fc epsilon receptor. Immunol. Rev. **217:**231–254.
2. **Anderson, D. H., and P. M. Ismail.** 1998. v-*fps* causes transformation by inducing tyrosine phosphorylation and activation of the PDGFβ receptor. Oncogene **16:**2321–2331.
3. **Aspenstrom, P., A. Fransson, and N. Richnau.** 2006. Pombe Cdc15 homology proteins: regulators of membrane dynamics and the actin cytoskeleton. Trends Biochem. Sci. **31:**670–679.
4. **Balla, T., and P. Varnai.** 2002. Visualizing cellular phosphoinositide pools with GFP-fused protein-modules. Sci. STKE **2002:**PL3.
5. **Brooks-Wilson, A. R., E. Ball, and T. Pawson.** 1989. The myristylation signal of p60$^{v\text{-}src}$ functionally complements the N-terminal *fps*-specific region of P130$^{gag\text{-}fps}$. Mol. Cell. Biol. **9:**2214–2219.
6. **Brunati, A. M., R. Deana, A. Folda, M. L. Massimino, O. Marin, S. Ledro, L. A. Pinna, and A. Donella-Deana.** 2005. Thrombin-induced tyrosine phosphorylation of HS1 in human platelets is sequentially catalyzed by Syk and Lyn tyrosine kinases and associated with the cellular migration of the protein. J. Biol. Chem. **280:**21029–21035.
7. **Cheng, H., J. A. Rogers, N. A. Dunham, and T. E. Smithgall.** 1999. Regulation of c-Fes tyrosine kinase and biological activities by N-terminal coiled-coil oligomerization domains. Mol. Cell. Biol. **19:**8335–8343.
8. **Cheng, H. Y., A. P. Schiavone, and T. E. Smithgall.** 2001. A point mutation in the N-terminal coiled-coil domain releases c-Fes tyrosine kinase activity and survival signaling in myeloid leukemia cells. Mol. Cell. Biol. **21:**6170–6180.
9. **Chitu, V., and E. R. Stanley.** 2007. Pombe Cdc15 homology (PCH) proteins: coordinators of membrane-cytoskeletal interactions. Trends Cell Biol. **17:**145–156.
10. **Craig, A., and P. Greer.** 2002. Fer kinase is required for sustained p38 kinase activation and maximal chemotaxis of activated mast cells. Mol. Cell. Biol. **22:**6363–6374.
11. **Craig, A. W., R. Zirngibl, K. Williams, L. A. Cole, and P. A. Greer.** 2001. Mice devoid of Fer protein-tyrosine kinase activity are viable and fertile but display reduced cortactin phosphorylation. Mol. Cell. Biol. **21:**603–613.
12. **Craig, A. W. B., R. Zirngibl, and P. Greer.** 1999. Disruption of coiled-coil domains in Fer protein-tyrosine kinase abolishes trimerization but not kinase activation. J. Biol. Chem. **274:**19934–19942.
13. **Dawicki, W., and J. S. Marshall.** 2007. New and emerging roles for mast cells in host defence. Curr. Opin. Immunol. **19:**31–38.
14. **Filippakopoulos, P., M. Kofler, O. Hantschel, G. D. Gish, F. Grebien, E. Salah, P. Neudecker, L. E. Kay, B. E. Turk, G. Superti-Furga, T. Pawson, and S. Knapp.** 2008. Structural coupling of SH2-kinase domains links Fes and Abl substrate recognition and kinase activation. Cell **134:**793–803.
15. **Franchini, G., J. Even, C. J. Sherr, and F. Wong-Staal.** 1981. *onc* sequences (v-*fes*) of Snyder-Theilen feline sarcoma virus are derived from noncontiguous regions of a cat cellular gene (c-*fes*). Nature **290:**154–157.
16. **Frost, A., R. Perera, A. Roux, K. Spasov, O. Destaing, E. H. Egelman, P. De Camilli, and V. M. Unger.** 2008. Structural basis of membrane invagination by F-BAR domains. Cell **132:**807–817.
17. **Fukamachi, H., N. Yamada, T. Miura, T. Kato, M. Ishikawa, E. Gulbins, A. Altman, Y. Kawakami, and T. Kawakami.** 1994. Identification of a protein, SPY75, with repetitive helix-turn-helix motifs and an SH3 domain as a major substrate for protein tyrosine kinase(s) activated by Fc epsilon RI cross-linking. J. Immunol. **152:**642–652.
18. **Gomez, T. S., S. D. McCarney, E. Carrizosa, C. M. Labno, E. O. Comiskey, J. C. Nolz, P. Zhu, B. D. Freedman, M. R. Clark, D. J. Rawlings, D. D. Billadeau, and J. K. Burkhardt.** 2006. HS1 functions as an essential actin-regulatory adaptor protein at the immune synapse. Immunity **24:**741–752.
19. **Greer, P.** 2002. Closing in on the biological functions of Fps/Fes and Fer. Nat. Rev. Mol. Cell Biol. **3:**278–289.
20. **Gregory, G. D., and M. A. Brown.** 2006. Mast cells in allergy and autoimmunity: implications for adaptive immunity. Methods Mol. Biol. **315:**35–50.
21. **Grimbaldeston, M. A., M. Metz, M. Yu, M. Tsai, and S. J. Galli.** 2006. Effector and potential immunoregulatory roles of mast cells in IgE-associated acquired immune responses. Curr. Opin. Immunol. **18:**751–760.

22. **Hackenmiller, R., J. Kim, R. A. Feldman, and M. C. Simon.** 2000. Abnormal Stat activation, hematopoietic homeostasis, and innate immunity in c-*fes*$^{-/-}$ mice. Immunity **13:**397–407.
23. **Hao, J. J., G. B. Carey, and X. Zhan.** 2004. Syk-mediated tyrosine phosphorylation is required for the association of hematopoietic lineage cell-specific protein 1 with lipid rafts and B cell antigen receptor signalosome complex. J. Biol. Chem. **279:**33413–33420.
24. **Hao, J. J., J. Zhu, K. Zhou, N. Smith, and X. Zhan.** 2005. The coiled-coil domain is required for HS1 to bind to F-actin and activate Arp2/3 complex. J. Biol. Chem. **280:**37988–37994.
25. **Hawley, R. G., F. H. Lieu, A. Z. Fong, and T. S. Hawley.** 1994. Versatile retroviral vectors for potential use in gene therapy. Gene Ther. **1:**136–138.
26. **Heath, R. J., and R. H. Insall.** 2008. Dictyostelium MEGAPs: F-BAR domain proteins that regulate motility and membrane tubulation in contractile vacuoles. J. Cell Sci. **121:**1054–1064.
27. **Henne, W. M., H. M. Kent, M. G. Ford, B. G. Hegde, O. Daumke, P. J. Butler, R. Mittal, R. Langen, P. R. Evans, and H. T. McMahon.** 2007. Structure and analysis of FCHo2 F-BAR domain: a dimerizing and membrane recruitment module that effects membrane curvature. Structure **15:**839–852.
28. **Hernandez-Hansen, V., A. J. Smith, Z. Surviladze, A. Chigaev, T. Mazel, J. Kalesnikoff, C. A. Lowell, G. Krystal, L. A. Sklar, B. S. Wilson, and J. M. Oliver.** 2004. Dysregulated FcεRI signaling and altered Fyn and SHIP activities in Lyn-deficient mast cells. J. Immunol. **173:**100–112.
29. **Hornstein, I., A. Alcover, and S. Katzav.** 2004. Vav proteins, masters of the world of cytoskeleton organization. Cell Signal. **16:**1–11.
30. **Huang, H., L. Li, C. Wu, D. Schibli, K. Colwill, S. Ma, C. Li, P. Roy, K. Ho, Z. Songyang, T. Pawson, Y. Gao, and S. S. Li.** 2008. Defining the specificity space of the human Src-homology 2 domain. Mol. Cell Proteomics **7:**768–784.
31. **Huang, S., L. Lifshitz, V. Patki-Kamath, R. Tuft, K. Fogarty, and M. P. Czech.** 2004. Phosphatidylinositol-4,5-bisphosphate-rich plasma membrane patches organize active zones of endocytosis and ruffling in cultured adipocytes. Mol. Cell. Biol. **24:**9102–9123.
32. **Huynh, H., N. Bottini, S. Williams, V. Cherepanov, L. Musumeci, K. Saito, S. Bruckner, E. Vachon, X. Wang, J. Kruger, C. W. Chow, M. Pellecchia, E. Monosov, P. A. Greer, W. Trimble, G. P. Downey, and T. Mustelin.** 2004. Control of vesicle fusion by a tyrosine phosphatase. Nat. Cell Biol. **6:**831–839.
33. **Itoh, T., K. S. Erdmann, A. Roux, B. Habermann, H. Werner, and P. De Camilli.** 2005. Dynamin and the actin cytoskeleton cooperatively regulate plasma membrane invagination by BAR and F-BAR proteins. Dev. Cell **9:**791–804.
34. **Kalesnikoff, J., E. J. Rios, C. C. Chen, M. Alejandro Barbieri, M. Tsai, S. Y. Tam, and S. J. Galli.** 2007. Roles of RabGEF1/Rabex-5 domains in regulating FcεRI surface expression and FcεRI-dependent responses in mast cells. Blood **109:**5308–5317.
35. **Kalesnikoff, J., E. J. Rios, C. C. Chen, S. Nakae, B. A. Zabel, E. C. Butcher, M. Tsai, S. Y. Tam, and S. J. Galli.** 2006. RabGEF1 regulates stem cell factor/c-Kit-mediated signaling events and biological responses in mast cells. Proc. Natl. Acad. Sci. USA **103:**2659–2664.
36. **Kim, L., and T. W. Wong.** 1995. The cytoplasmic tyrosine kinase FER is associated with the catenin-like substrate pp120 and is activated by growth factors. Mol. Cell. Biol. **15:**4553–4561.
37. **Laurent, C. E., F. J. Delfino, H. Y. Cheng, and T. E. Smithgall.** 2004. The human c-Fes tyrosine kinase binds tubulin and microtubules through separate domains and promotes microtubule assembly. Mol. Cell. Biol. **24:**9351–9358.
38. **Martinez-Quiles, N., H. Y. Ho, M. W. Kirschner, N. Ramesh, and R. S. Geha.** 2004. Erk/Src phosphorylation of cortactin acts as a switch on-switch off mechanism that controls its ability to activate N-WASP. Mol. Cell. Biol. **24:**5269–5280.
39. **Maurer, M., J. Wedemeyer, M. Metz, A. M. Piliponsky, K. Weller, D. Chatterjea, D. E. Clouthier, M. M. Yanagisawa, M. Tsai, and S. J. Galli.** 2004. Mast cells promote homeostasis by limiting endothelin-1-induced toxicity. Nature **432:**512–516.
40. **McCafferty, D. M., A. W. Craig, Y. A. Senis, and P. A. Greer.** 2002. Absence of Fer protein-tyrosine kinase exacerbates leukocyte recruitment in response to endotoxin. J. Immunol. **168:**4930–4935.
41. **Metz, M., and M. Maurer.** 2007. Mast cells–key effector cells in immune responses. Trends Immunol. **28:**234–241.
42. **Metz, M., A. M. Piliponsky, C. C. Chen, V. Lammel, M. Abrink, G. Pejler, M. Tsai, and S. J. Galli.** 2006. Mast cells can enhance resistance to snake and honeybee venoms. Science **313:**526–530.
43. **Morita, Y., and R. P. Siraganian.** 1981. Inhibition of IgE-mediated histamine release from rat basophilic leukemia cells and rat mast cells by inhibitors of transmethylation. J. Immunol. **127:**1339–1344.
44. **Naba, A., C. Reverdy, D. Louvard, and M. Arpin.** 2008. Spatial recruitment and activation of the Fes kinase by ezrin promotes HGF-induced cell scattering. EMBO J. **27:**38–50.
45. **Nishida, K., S. Yamasaki, Y. Ito, K. Kabu, K. Hattori, T. Tezuka, H. Nishizumi, D. Kitamura, R. Goitsuka, R. S. Geha, T. Yamamoto, T. Yagi, and T. Hirano.** 2005. FcεRI-mediated mast cell degranulation requires calcium-independent microtubule-dependent translocation of granules to the plasma membrane. J. Cell Biol. **170:**115–126.
46. **Odom, S., G. Gomez, M. Kovarova, Y. Furumoto, J. J. Ryan, H. V. Wright, C. Gonzalez-Espinosa, M. L. Hibbs, K. W. Harder, and J. Rivera.** 2004. Negative regulation of immunoglobulin E-dependent allergic responses by Lyn kinase. J. Exp. Med. **199:**1491–1502.
47. **Papayannopoulos, V., C. Co, K. E. Prehoda, S. Snapper, J. Taunton, and W. A. Lim.** 2005. A polybasic motif allows N-WASP to act as a sensor of PIP(2) density. Mol. Cell **17:**181–191.
48. **Parsons, S. A., and P. A. Greer.** 2006. The Fps/Fes kinase regulates the inflammatory response to endotoxin through down-regulation of TLR4, NF-κB activation, and TNF-α secretion in macrophages. J. Leukoc. Biol. **80:**1522–1528.
49. **Pivniouk, V. I., S. B. Snapper, A. Kettner, H. Alenius, D. Laouini, H. Falet, J. Hartwig, F. W. Alt, and R. S. Geha.** 2003. Impaired signaling via the high-affinity IgE receptor in Wiskott-Aldrich syndrome protein-deficient mast cells. Int. Immunol. **15:**1431–1440.
50. **Qi, W., K. V. Ebbert, A. W. Craig, P. A. Greer, and D. M. McCafferty.** 2005. Absence of Fer protein tyrosine kinase exacerbates endotoxin induced intestinal epithelial barrier dysfunction in vivo. Gut **54:**1091–1097.
51. **Rivera, J., and A. M. Gilfillan.** 2006. Molecular regulation of mast cell activation. J. Allergy Clin. Immunol. **117:**1214–1225, 1226.
52. **Rivera, J., and A. Olivera.** 2007. Src family kinases and lipid mediators in control of allergic inflammation. Immunol. Rev. **217:**255–268.
53. **Sangrar, W., Y. Gao, M. Scott, P. Truesdell, and P. A. Greer.** 2007. Fer-mediated cortactin phosphorylation is associated with efficient fibroblast migration and is dependent on reactive oxygen species generation during integrin-mediated cell adhesion. Mol. Cell. Biol. **27:**6140–6152.
54. **Schwede, T., J. Kopp, N. Guex, and M. C. Peitsch.** 2003. SWISS-MODEL: an automated protein homology-modeling server. Nucleic Acids Res. **31:**3381–3385.
55. **Senis, Y. A., A. W. Craig, and P. A. Greer.** 2003. Fps/Fes and Fer protein-tyrosine kinases play redundant roles in regulating hematopoiesis. Exp. Hematol. **31:**673–681.
56. **Sherr, C. J., L. A. Fedele, M. Oskarsson, J. Maizel, and G. V. Woude.** 1980. Molecular cloning of Snyder-Theilen feline leukemia and sarcoma viruses: comparative studies of feline sarcoma virus with its natural helper virus and with Moloney murine sarcoma virus. J. Virol. **34:**200–212.
57. **Shibuya, M., and H. Hanafusa.** 1982. Nucleotide sequence of Fujinami sarcoma virus: evolutionary relationship of its transforming gene with transforming genes of other sarcoma viruses. Cell **30:**787–795.
58. **Shibuya, M., T. Hanafusa, H. Hanafusa, and J. R. Stephenson.** 1980. Homology exists among the transforming sequences of avian and feline sarcoma viruses. Proc. Natl. Acad. Sci. USA **77:**6536–6540.
59. **Shimada, A., H. Niwa, K. Tsujita, S. Suetsugu, K. Nitta, K. Hanawa-Suetsugu, R. Akasaka, Y. Nishino, M. Toyama, L. Chen, Z. J. Liu, B. C. Wang, M. Yamamoto, T. Terada, A. Miyazawa, A. Tanaka, S. Sugano, M. Shirouzu, K. Nagayama, T. Takenawa, and S. Yokoyama.** 2007. Curved EFC/F-BAR-domain dimers are joined end to end into a filament for membrane invagination in endocytosis. Cell **129:**761–772.
60. **Sivalenka, R. R., and R. Jessberger.** 2004. SWAP-70 regulates c-kit-induced mast cell activation, cell-cell adhesion, and migration. Mol. Cell. Biol. **24:**10277–10288.
61. **Songyang, Z., K. L. Carraway III, M. J. Eck, S. C. Harrison, R. A. Feldman, M. Mohammadi, J. Schlessinger, S. R. Hubbard, D. P. Smith, C. Eng, and et al.** 1995. Catalytic specificity of protein-tyrosine kinases is critical for selective signalling. Nature **373:**536–539.
62. **Songyang, Z., S. E. Shoelson, J. McGlade, P. Olivier, T. Pawson, X. R. Bustelo, M. Barbacid, H. Sabe, H. Hanafusa, T. Yi, et al.** 1994. Specific motifs recognized by the SH2 domains of Csk, 3BP2, fps/fes, GRB-2, HCP, SHC, Syk, and Vav. Mol. Cell. Biol. **14:**2777–2785.
63. **Stone, J. C., T. Atkinson, M. Smith, and T. Pawson.** 1984. Identification of functional regions in the transforming protein of Fujinami sarcoma virus by in-phase insertion mutagenesis. Cell **37:**549–558.
64. **Takahashi, S., R. Inatome, A. Hotta, Q. Qin, R. Hackenmiller, M. C. Simon, H. Yamamura, and S. Yanagi.** 2003. Role for Fes/Fps tyrosine kinase in microtubule nucleation through is Fes/CIP4 homology domain. J. Biol. Chem. **278:**49129–49133.
65. **Tam, S. Y., M. Tsai, J. N. Snouwaert, J. Kalesnikoff, D. Scherrer, S. Nakae, D. Chatterjea, D. M. Bouley, and S. J. Galli.** 2004. RabGEF1 is a negative regulator of mast cell activation and skin inflammation. Nat. Immunol. **5:**844–852.
66. **Tsujita, K., S. Suetsugu, N. Sasaki, M. Furutani, T. Oikawa, and T. Takenawa.** 2006. Coordination between the actin cytoskeleton and membrane deformation by a novel membrane tubulation domain of PCH proteins is involved in endocytosis. J. Cell Biol. **172:**269–279.
67. **Udell, C. M., L. A. Samayawardhena, Y. Kawakami, T. Kawakami, and A. W. Craig.** 2006. Fer and Fps/Fes participate in a Lyn-dependent pathway from FcεRI to platelet-endothelial cell adhesion molecule 1 to limit mast cell activation. J. Biol. Chem. **281:**20949–20957.

68. **Uruno, T., J. Liu, Y. Li, N. Smith, and X. Zhan.** 2003. Sequential interaction of actin-related proteins 2 and 3 (Arp2/3) complex with neural Wiscott-Aldrich syndrome protein (N-WASP) and cortactin during branched actin filament network formation. J. Biol. Chem. **278:**26086–26093.
69. **Xiao, W., H. Nishimoto, H. Hong, J. Kitaura, S. Nunomura, M. Maeda-Yamamoto, Y. Kawakami, C. A. Lowell, C. Ra, and T. Kawakami.** 2005. Positive and negative regulation of mast cell activation by Lyn via the FcεRI. J. Immunol. **175:**6885–6892.
70. **Zerial, M., and H. McBride.** 2001. Rab proteins as membrane organizers. Nat. Rev. Mol. Cell Biol. **2:**107–117.
71. **Zirngibl, R., D. Schulze, S. E. Mirski, S. P. Cole, and P. A. Greer.** 2001. Subcellular localization analysis of the closely related Fps/Fes and Fer protein-tyrosine kinases suggests a distinct role for Fps/Fes in vesicular trafficking. Exp. Cell Res. **266:**87–94.
72. **Zirngibl, R. A., Y. Senis, and P. A. Greer.** 2002. Enhanced endotoxin sensitivity in fps/fes-null mice with minimal defects in hematopoietic homeostasis. Mol. Cell. Biol. **22:**2472–2486.